Role of Cytoplasmic Dyneins in Neuronal Force Generation

B.S – M.S Thesis

P S Lakshmi

20111015

Under the guidance of

Dr. Aurnab Ghose

IISER Pune

Certificate

This is to certify that this dissertation entitled “Role of Cytoplasmic Dyneins in Neuronal Force Generation” towards the partial fulfilment of the B.S - M.S dual degree programme at the Indian Institute of Science Education and Research, Pune represents the research carried out by P S Lakshmi at IISER Pune under the supervision of Dr. Aurnab Ghose, Associate Professor, IISER Pune during the academic year 2015-2016.

Date: 2016 – 03 - 28

Dr. Aurnab Ghose,

Associate Professor,

IISER Pune.

Declaration

I hereby declare that the matter embodied in the report entitled “Role of Cytoplasmic Dyneins in Neuronal Force Generation” are the results of the investigations carried out by me at the Department of Biology, IISER Pune, under the supervision of Dr. Aurnab Ghose and the same has not been submitted elsewhere for any other degree.

Date: 2016 – 03 – 28

P S Lakshmi

20111015

B.S – M.S Student

IISER Pune

Abstract

Cytoplasmic dynein is a motor protein classically involved in transport of cargo towards the minus end of microtubules. This project focuses on the role of dynein in forward translocation of cytoskeletal meshwork in growth cones. This pushing action of dynein, which is antagonistic to the pulling action of contractile myosin II in the growth cone, help balance forces in the growth cone to aid in its forward translocation. Many mechanisms have been proposed to explain how dynein telescopes microtubules towards the growth cone periphery, hence creating a pushing force. But there is no systematic study proving any of these mechanisms. Also, there are no quantitative studies that measure forces exerted by dynein in pushing membranes. This project uses a filopodial bead pulling assay to calculate quantitatively the filopodial contractility upon inhibition of dynein. The study shows that dynein inhibition maintains filopodial contractility in terms of pull step size and velocity but the frequency of pulls per unit time is observed to increases. A traction assay is also employed to qualitatively state that the traction is lower in dynein depleted neurons. This decrease in traction force exerted on the substrate in dynein inhibited neurons is substantiated by a showing that the point contacts are weaker in dynein disrupted conditions. Put together, we propose that when dynein is inhibited in neurons, the force balance will be tipped in favor of myosin, which could transiently increase the traction. Weaker point contacts in these neurons start detaching from the substrate soon after myosin takes over, hence conveying a decrease in the traction exerted on the substrate and a consequent stalling of the growth cone.

.

Table of Contents:

Chapter 1: Introduction……..01

1.1 Structure of a growth cone……...01

1.2 Point contacts and their dynamics……02

1.3 Force generation at point contacts……...04

1.4 Force balance in neurons……..05

1.4.1 The push of cytoplasmic dyneins……05

1.4.2 The pull of Myosin II……07

1.5 Dynein and point contacts……..08

1.6 Objectives and approach……09

Chapter 2: Materials and Methods……..11

2.1 Materials……..11

2.2 Methods……...11

2.2.1 Functionalization of coverslips……11

2.2.2 Polyacrylamide (PAA) hydrogel preparation and ECM crosslinking…..12

2.2.3 Dissection and Culturing……...13

2.2.4 Morphology analysis of Cilio D treated growth cones……...13

2.2.5 Bead Pulling Assay……14

2.2.6 Traction force assay……...16

2.2.7 Phospho – FAK Staining……18

2.2.8 Phospho-FAK Quantification……19

2.2.9 Cloning of xMRLC into a pCAG backbone and expression……19

Chapter 3: Results……21

3.1 Reduction in number of filopodia per growth cone upon dynein disruption……..21

3.2 Reduction in the growth cone area upon dynein disruption……..22

3.3 Dynein disruption does not alter magnitude or velocity of filopodial pulling..…...22

3.4 Dynein disruption increases the number of filopodial pulling events……....23

3.5 Traction force assay qualitatively shows lower traction upon dynein disruption..25

3.6 Intensity of P-FAK staining is lower in dynein inhibited growth cones……..…26

3.7 Cloning and expression of Myosin Regulatory Light Chain (MRLC)……..27

Chapter 4: Conclusions and Discussion……...31

4.1 Cilio D Activity is confirmed in chick spinal neuronal cultures… ……31

4.2 Dynein inhibition maintains filopodial pull step sizes and velocities, but increases the pull frequency per unit time ……31

4.3 Dynein inhibited growth cones show a qualitative decrease in traction forces exerted on the substrate ……..32

4.4 Dynein inhibited growth cones have weaker point contacts.....32

References……34

List of Figures

Figure 1.1: Structure of a neuron and a growth cone……..…….……2

Figure 1.2: Localization of point contacts in neurons…….……...……3

Figure 1.3: Motor clutch force transmission system for substrate sensing……...……4

Figure 1.4: Structure of cytoplasmic dynein……..……..…5

Figure 1.5: Possible mechanisms by which dynein moves microtubules anterogradely.7

Figure 2.1 Cartoon representation and real images of filopodial pulling and analysis....16

Figure 2.2 Growth cone area estimation and cartoons for traction force microscopy…18

Figure 3.1: Reduction in number of filopodia per growth cone upon dynein disruption.21

Figure 3.2: Reduction in the growth cone area upon dynein disruption....……...…23

Figure 3.3: Analysis of Bead pulling assay for DMSO and Cilio D treated filopodia…..24

Figure 3.4: Pulling frequencies of filopodial tips increase upon disruption of dynein….25

Figure 3.5: Traction force images of neurons……..…….26

Figure 3.6: Phospho-FAK Staining in neurons after drug treatment (Cilio D/ DMSO)...28

Figure 3.7: Phospho-FAK intensity quantification in DMSO, Cilio D treated cells……..29

Figure 3.8: xMRLC cloning and expression in chick spinal neurons…….……..…..30

Acknowledgements

First and foremost, I thank Dr. Aurnab Ghose for his encouragement throughout the project tenure. He boosted up my morale and kept me motivated during multiple contamination eras. I am also very grateful to Sampada, who has been of immense help, be it teaching protocols, finding literature, frequent discussions or keeping things organized. I thank Abhishek and Ketakee, for being excellent libraries whenever anything was required. I also thank Tanushree, for her willingness to help, for all the meaningful discussions and mostly, for being so curious and interested in my project. I thank Ajesh for his help with all the cloning. I also thank Dhriti and Priyanka for moral support and for creating a happy atmosphere to work in.

I am very grateful to my parents for being very understanding throughout this journey. I can't thank them enough for all the late night reassurances and for being my wake up alarm every day. Thanks Devu, for being by me at all times, for keeping me happy. I also thank my grandmother for showering on me so much unconditional grandma love.

Chapter – 1

Introduction

Structure of a growth cone:

Environmental sensing is extremely important during the development of neurons, since precise neuronal connections are essential to build functional circuits. Growth cones, implicated in sensing the environment, are dynamic structures seen at the terminals of axons consisting of lamellipodial and filopodial structures (Figure 1.1 A and B). Filopodia are the 'antennae' of growth cones which, in addition to being sensors, are involved in advancement of growth cone (Mattila, P.K. et al. 2008). The two key cytoskeletal elements of a neuron are actin and microtubules. A network of branched actin filaments are present in the lamellipodia and bundled actin is present in the filopodia (Figure 1.1 B), (Lowery, et al. 2009). Microtubules are oriented with their plus ends towards the growth cone leading edge (Heidemann et al. 1981) and the microtubule bundles and are present along the axon shaft and in the filopodia (Figure 1.1 (B)), where they are implicated in pushing the membrane to aid in moving forward (Lu, et al. 2013). Growth cones respond to guidance cues by reorganizing their cytoskeleton and moving towards attractive cues and being repelled by repulsive cues. Actin forms filaments called F-actin and these polymerize by adding the monomers Globular- actin (G-actin) at the barbed end of the filament. The constant addition of monomers at the barbed end and depolymerization at the other end is called treadmilling. At any given time, F-actin retrograde flow and F-actin treadmilling decide whether a filopodia advances or withdraws (Lowery et al. 2009). A steady F-actin retrograde flow is always there toward the centre of the growth cone (Zhang et al. 2003), which is driven by contractile activity of myosin II at the T zone and by the push generated due to F-actin treadmilling in the P-zone (Medeiros et al. 2006).

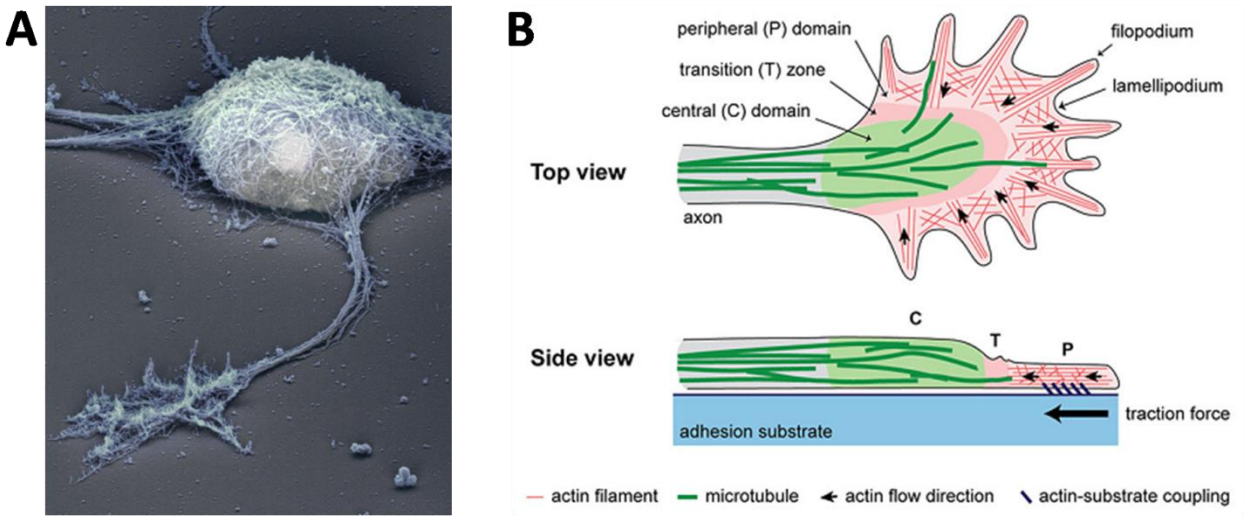

Figure 1.1: Structure of a neuron and a growth cone. (A) shows an electron microscopic image of a neuron devoid of its cell membrane, showing cytoskeletal structures. Adapted from Google images, clicked by Bernd Knöll (University of Tübingen), Jürgen Berger, and Heinz Schwarz (Max Planck Institute for Developmental Biology). (B) Adapted from Athamneh et al. 2015, this image shows the top and side view of a labeled growth cone, highlighting the actin and microtubule structures inside. It also shows the coupling between the F-actin in the filopodia and the substrate, and generation of traction forces.

Point contacts and their dynamics:

Growth cones have small adhesive point contacts, analogous in function to the large focal adhesions seen in non-neuronal cells (Gomez, et al. 1996). The point contacts are punctate structures seen all over the growth cone (Figure1.2 A) (Robles and Gomez, 2006, Gomez et al. 1996, Wu et al 1993). A point contact recruits many proteins for maturation, some of which are vinculin, paxillin, talin, Focal adhesion Kinase (FAK), Src, etc (Figure 1.2 (B)). FAKs are one of the signaling proteins that are necessarily recruited in neurons to point contacts, and this causes autophosphorylation of FAK at many places including Y397, after which it becomes active. This Phospho-FAK (P-FAK) is enriched in point contacts that are also enriched in phospho-tyrosine (PY) (Robles and Gomez, 2006) (Figure 1.2 A), whose accumulation at filopodial tips has been shown to bring about filopodial elongation (Robles et al. 2005). Reduced growth cone motility on fibronectin substrate as opposed to a laminin substrate has been shown to

be because of the point contacts being fewer in number, larger and more stable on fibronectin as compared to laminin. The small, punctuate and dynamic structures on laminin substrate indicate that higher number of point contacts, along with a higher turnover rate promotes growth cone migration (Robles and Gomez, 2006). It has also been observed that PY co-localizes with the FAK and Paxillin in all regions in the growth cone, except the filopodial tip. The filopodial tip contains only PY and this suggests that there is no stable adhesion point at the tips (Robles and Gomez, 2006 and Myers et al. 2011).

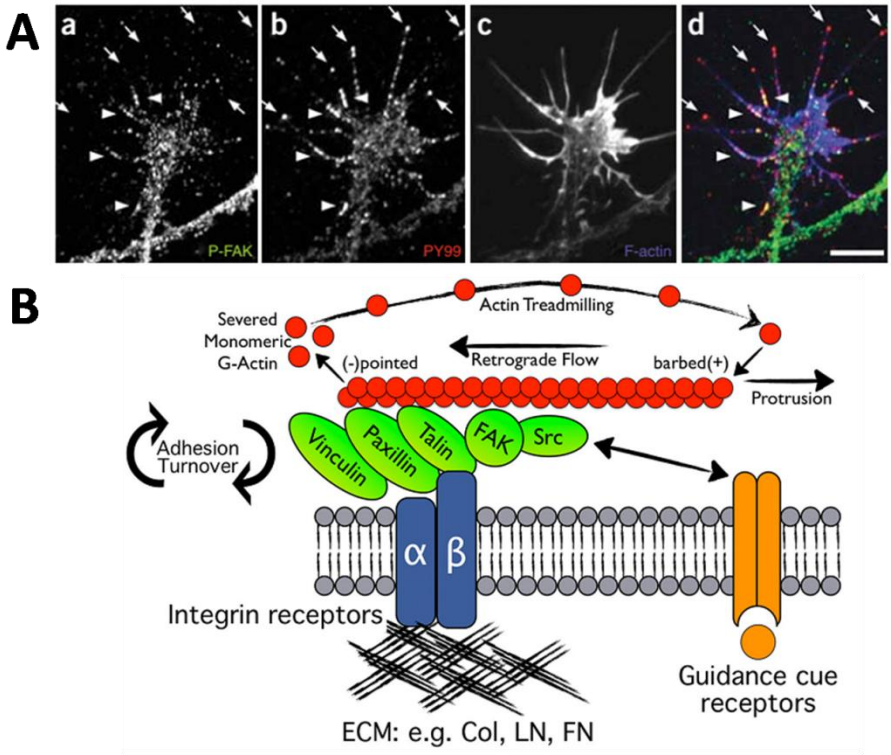

Figure 1.2: Localization of point contacts in neurons. (A) shows how P-FAK colocalizes with PY99 everywhere else except at the filopodial tips. It also shows that point contacts are formed all over the growth cone, even the filopodial tips. Adapted from Robles and Gomez, 2006. (B) shows a cartoon of a stabilized point contact in a growth cone showing the key partners. Adapted from Myers et. al. 2011.

Force generation at point contacts

A focal point is created due to coupling of F-actin to the substrate via molecular clutches. This is called a motor- clutch force transmission system as described by Chan and Odde, 2008. This model consists of myosin motors pulling onto the F-actin as it is engaging with molecular clutches attaching to the substrate (Figure 1.3 A). If there is enough tension generated along the clutches, traction is generated, the retrograde flow slows down and the balance is tipped towards F-actin polymerization. Chan and Odde, 2008 have showed that on a compliant substrate, where the molecular clutches can attach longer until they break, this scenario, called 'load and fail' mechanism happens. Hence, if the coupling is tighter, protrusions on filopodia occur (Suter and Forscher, 2001). On the contrary, a stiff substrate would cause the clutches to break very soon, and hence enough traction is not generated for translocation. Also, since there is no significant pull by the clutch, the retrograde flow remains unaffected (Chan and Odde, 2008).

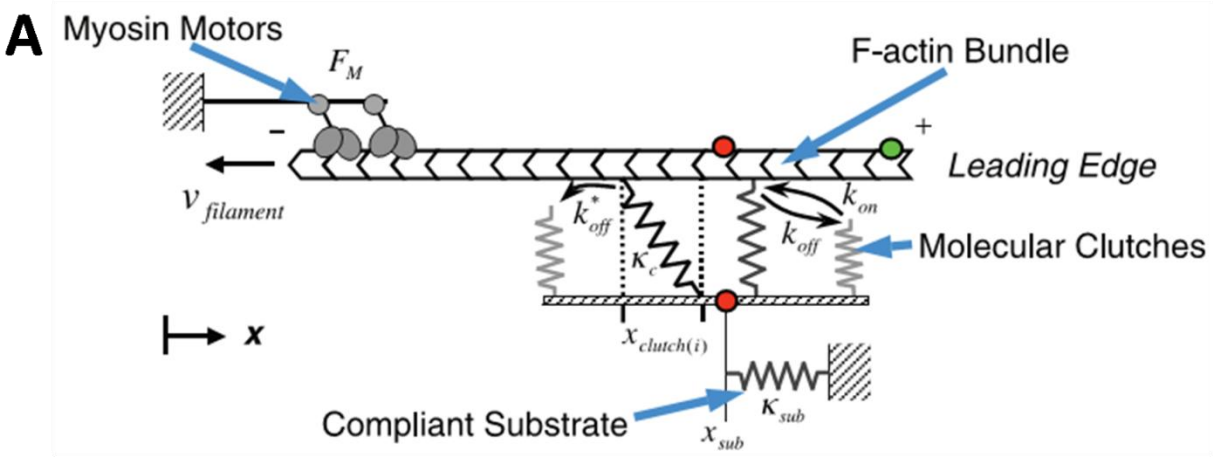

Figure 1.3: Motor clutch force transmission system for substrate sensing. (A) shows various forces actin on an F-actin filament: Myosin motors pulling it towards the cell body, molecular clutches trying to restrain it and actin polymerization at the barbed end. Adapted from Chan and Odde, 2008.

Force balance in neurons:

1. **The push of cytoplasmic dyneins:**

Dyneins belong to AAA+ ATPase (ATPases Associated with diverse cellular Activities) family, and consist of a cargo binding domain, two motor heads and two microtubule binding domains (Gennerich and Vale, 2009, Schnapp and Reese et al. 1989) as shown in Figures 1.4 A, B. In neurons, dynein is localized in the leading edge of the growth cone and in the soma (Tsai et al 2007). The motor heads contain multiple AAA+ ATP binding sites. Dyneins are classically known for their role in transport of cargo towards the minus end of microtubules, mechanisms of which have been described in Gennerich and Vale, 2009. Dynein is also implicated in various other functions such as cell migration and mitotic spindle formation (Firestone et al. 2012).

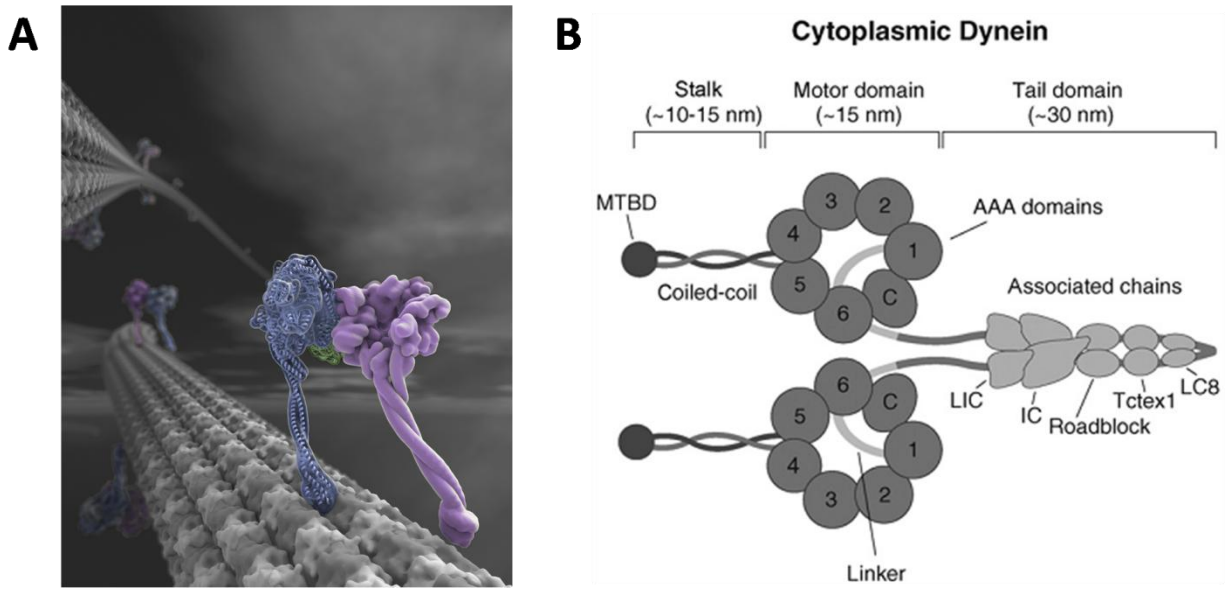

Figure 1.4: Structure of cytoplasmic dynein. Adapted from Google images, (A) shows an artwork by Graham Johnson, of dynein moving on microtubules, based on the crystal structure described by Carter et al. 2011. (B) shows a cartoon representation of the structure of cytoplasmic dynein, showing various domains. Adapted from Gennerich and Vale, 2009.

Dynein knockdown/ inhibition assays have established that in addition to dynein being required for proper growth cone turning (Myers et al. 2006), proper arborization and targeting of axons (Murphey et al. 1999), it is also required for proper positioning of microtubules in the filopodia (Myers et al. 2006, Castillo et al. 2015) and in the axon (Ahmad et al. 1998), anterograde movement of microtubules (He et al. 2005), growth cone advance (Abe et al. 2008), proper axonal outgrowth (Grabham et al. 2007, Ahmad et al. 2006), maintenance of both axonal lengths (Ahmad et al. 2006, Sainath et al. 2014, Roossien et al. 2014), filopodial numbers (Sainath et al. 2014) and NGF induced formation of axonal filopodia (Sainath et al. 2014).

Since dynein is involved in growth cone translocation forward, axon extension, proper arborization, neurite outgrowth and translocation of microtubule array as mentioned above, dynein is thought to push the cytoskeletal meshwork in an anterograde direction (Roossien et al. 2014, Dehmelt et al. 2006).

A lot of mechanisms that have been put forth to explain this. Dehmelt et al. 2006 puts forward the possibility that the cargo domain of microtubules could be linked to a non polar, non directional scaffold (such as long microtubules, actin, etc.) and the huge inertia of this huge structure for movement could cause dynein to be fixed in space, while it is traversing on the short microtubules. This process effectively appear as though dynein is pushing the microtubule anterogradely (Figure 1.5 A). He et al. 2005 also discusses the same hypothesis to explain the role of dynein in anterograde microtubule transport as above, and they call it the sliding filament model. Roossien et al. 2014 postulates additionally that dynein could use cortical actin to push microtubules anterogradely, or plasma membrane anchored dynein could move microtubules anterogradely independent of cortical actin (Figure 1.5 A).

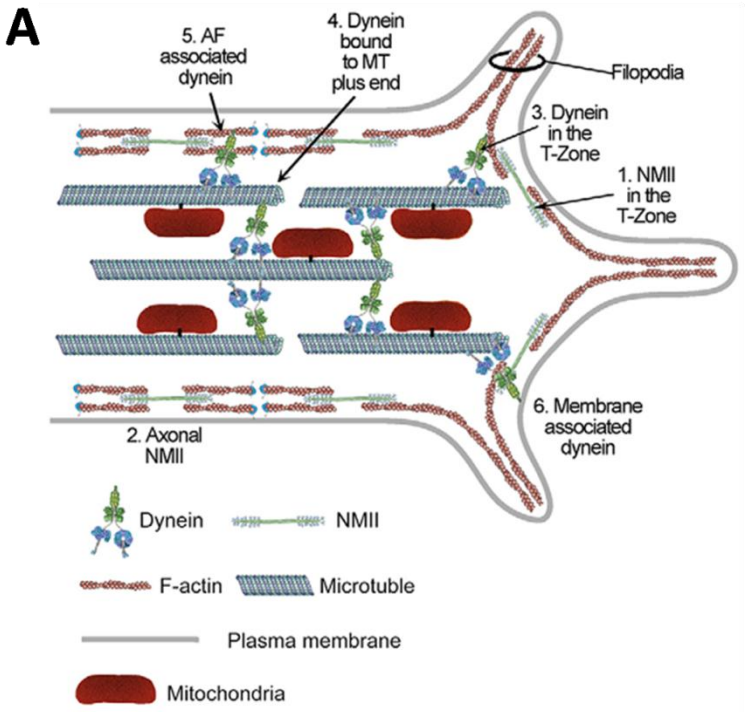

Figure 1.5: Possible mechanisms by which dynein moves microtubules anterogradely. (A) describes various ways by which dynein can bring about microtubule pushing, including dynein's use of either cortical actin/ actin in T-zone to push microtubules forward, or plasma membrane associated dynein in the axon/ growth cone directly moving microtubules forward independent of cortical actin. Adapted from Roossien et al 2014.

2. The pull of Myosin II:

Myosins are motor proteins that traverse on F-actin. Myosin II is localized at the interface between P and C domains of growth cones in the shape of an arc (Bridgman et al. 1980, Bridgman et al. 2001, Rochlin et al. 1995, Medeiros et al. 2006), where they apply their contractile forces act on F-actin, pulling the actin mesh towards the C-domain (Lin et al. 1996, Roossien et al. 2014). Myosin II is also involved in generation of traction in growth cones (Bridgman et al. 2001).

Since myosin II applies a contractile force on the growth cone (towards the cell body), and dynein pushes microtubules toward the filopodia, these are antagonistic forces (Myers et al. 2006, Roossien et al. 2014, Hasaka et al. 2004, Ahmad et al. 2000) that work together to bring about growth cone motility.

Dynein and point contacts

Roossien et al. 2014 show that acute disruption of dynein causes an intital retraction of the actin meshwork from the periphery of the growth cone and hence reduced axon lengths, after which the growth cones stalls. Sainath et al. 2014 also see a slight retraction upon dynein disruption. Dynein depleted neurons de-adhere faster when treated with nitric oxide (Myers et al. 2006). Roissen et al. 2014 observe that the transient retraction due to dynein disruption happens in an accordion-like fashion in the distal axon, which they attribute to bulk pulling of the cytoskeletal meshwork.

During a normal retraction, point contacts in a growth cone are all not disengaged at once, they are in fact, slowly de-adhered and hence, the tension in the growth cone is released slowly. Thus, the axon retracts linearly (Franze et al. 2009). The accordion-like retraction in case of disruption of dynein could be either because of weaker point contacts or them being fewer in number. Hence, the de-adhering in this case is faster, and it is almost as though the growth cone is snapping back. Further, in NRK (normal rat kidney epithelial) cells, dynein intermediate chain 2 is reported to have been bound to paxillin during migration and that it can alter the pace of cell migration (Rosse et al., 2012). Since dynein physically binds to paxillin, we assume dynein must also be associated with force generation.

The classical protein trafficking function of dynein has been extensively studied. The force generating function of dynein has been studied to a lower extent. There are no mechanistic models as of now to explain how dynein works, or the interaction of dynein with focal adhesion signaling molecules. There are only speculations in this field as of now. The speculations are not only about the mechanism of action of dynein, but also the localization of dynein while it is telescoping microtubules anterogradely. Due to lack of reagents that could acutely and locally disrupt dynein until recently, there are not many thorough studies on the force generation aspect of dyneins. In fact, there is no literature quantifying forces generated by dyneins.

Objectives:

Since dyneins are involved in pushing microtubules towards growth cone periphery, one aim of the project is to study dynein activity at these peripheral regions, which are the filopodia. A part of the project investigates the role of dynein in filopodial contractility and quantifies the same.

As shown in the previous section, it is well established in literature that dynein causes growth cones to retract. If there is an effect at the levels of the whole growth cone, then dynein must be acting to create forces not only in filopodia, but also in the central region of a growth cone. Hence, the other part of the project is aimed at studying the role of dynein in generation of traction forces at the level of a whole growth cone.

As pointed out in the previous section, Roossien et al. 2014 show that dynein inhibited growth cones retract in an accordion like motion. This sinusoidal motion of the axon indicates that the growth cone is probably not attached to the substrate. To investigate if this is true, point contacts intensities in dynein depleted growth cones are used to comment on the force generating ability of dyneins in growth cones.

Approach:

Chick (*Gallus gallus*) spinal neuronal cultures are used as the model system for this investigation.

Inhibition was used as the method to inactivate dynein in this study. The advantage of using an inhibitor are multifold. Conventional methods for dynein disruption include use of siRNA against dynein heavy chain (DHC), dynactin disruption, dynamitin (p150) overexpression, dominant negative constructs of DHC etc. These approaches of knocking down and overexpression are chronic and global. Hence, they could potentially affect the general health of neurons, as dynein is also involved in protein trafficking. Inhibition, on the other hand, allows for acute and localized inhibition of dynein function. Another attraction for inhibitors is that they can be washed out and hence rescue experiments can be carried out. Rescue experiments are always more convincing than just disruptions.

A small molecule inhibitor of cytoplasmic dyneins 1 and 2, Ciliobrevin D (Cilio D) (Firestone et al. 2012) has been employed in this study. Cilio D is a competitive inhibitor for ATP at its binding site in the dynein motor, and thus it works by increasing the time that dynein spends attached to the microtubule after the power stroke (Kikkawa, 2013). It inhibits the ATPase activity of dynein in a concentration dependent way, but does not affect the kinesin motor domains. It has also been shown that it does not broadly target all AAA+ family and also that it does not disrupt the association of ADP bound dynein and microtubules. Also, this drug has been accepted in literature (Sainath et al. 2014 and Roossien et al. 2014) and it shows defects at the level of growth cones comparable to other methods of dynein disruption (Firestone et al. 2012). Cilio D can hence be used as a effective inhibitor for dynein.

Chapter 2

Materials and Methods:

Materials:

24 mm (# 1.5) and 18 mm (# 1.5) circular coverslips (Bluestar), APMS (Aminopropyltrimethoxysilane, Sigma-Aldrich), 35 mm culture dishes (Laxbro manufacturing company), Glutaraldehyde (Sigma-Aldrich), Acrylamide and Bisacrylamide (Sigma-Aldrich), TEMED (N,N,N',N'-tetramethylethylenediamine, APS (Ammonium persulphate, Sigma Aldrich), Red fluorescent beads (200 nm diameter, Invitrogen), Sulpho-SANPAH (sufosuccinimidyl-6-(4-azido-2-nitrophenylamino)-hexanoate, ThermoFisher Scientific), HEPES, Fibronectin from bovine plasma (Sigma-Aldrich), L-15, Penstrep,Methocel (kindly provided from Dr. PramodPullarkat, Raman Research Institute, acquired from Colorcon), D-Glucose, HI FBS (Heat inactivated fetal bovine serum,1X Trypsin, 10X Trypsin (Sigma-Aldrich), 0.45 µm syringe filters (Axiva), Ciliobrevin D (Merck Millipore), NGF (Nerve growth factor 7S, Invitrogen), Anti-FAK (phosphor Y397) antibody (Abcam), Phalloidin 488 (Invitrogen).

Methods:

Functionalization of coverslips:

The method used here has been adapted from Aplin and Hughes, 1981. Coverslips of 24 mm diameter were washed in 1N Hydrochloric acid at 60^{o}C for around 4 hours to remove any grease, if present. They were next subjected to 0.5% APMS for 15 minutes while shaking, followed by thorough rinsing with distilled water and baking at 160^{o}C for 1 hour. These coverslips were then stuck on 35 mm cultures which had holes of 22 mm diameter drilled into them. Further, 0.5% Glutaraldehyde was added, incubated for 1 hour at room temperature, and water washes were given to remove molecules that were unbound.

Reactions involved:

APMS reacts with the hydroxyl (-OH) molecules formed on the surface of the coverglass (after acid washing), forming a lateral siloxane (Si-O-Si) network, which is oriented so that it's positively charged amine groups (–NH2+) are sticking out of the coverslip. These amine groups are aldehyde scavengers, and hence react with one aldehyde group of Glutaraldehyde, which is added subsequently. After the water washes, all unbound glutaraldehyde is removed and the unreacted aldehyde group of the bound glutaraldehydes stick out.

Polyacrylamide (PAA) hydrogel preparation and ECM crosslinking:

Bead coating on coverslips was done by adding 50 µl of a 1:100 (v/v) fluorescent bead solution (diluted in distilled water), to a dry acid washed coverslip (of diameter 18 mm). These coverslips are then centrifuged in a spin bucket centrifuge machine, at 3500 rpm for 10 min.

PAA solution was prepared with 3% Acrylamide, 0.1% Bis-acrylamide, 1/100 (v/v) APS, and 1/1000 (v/v) TEMED in distilled water, the fabrication of which has been adapted from Tse and Engler, 2010. The elastic modulus of the gels used have not been measured yet, but we will carry out either AFM or Bead Indentation methods in the future to check the same. 15 µl of this gel solution was added onto the activated coverslip of each 35 mm culture dish, and a bead coated 18 mm coverslip was carefully placed on it, with the bead coated surface facing the gel drop. The gel is allowed to polymerize for 5-10 min, after which the 18 mm coverslip is taken away with forceps. 150 µl of0.2 mg/ml sulpho-SANPAH (dissolved in 20 mM HEPES) was added to each gel and the culture dish was irradiated with 365 nm using a hand-UV for 1 hour. Following this, Sulpho-SANPAH was drained and multiple 20 mM HEPES washes were given to remove all the unbound sulpho-SANPAH molecules. 150 µl of 50 µg/ ml Fibronectin was then added to each plate and incubated at $4^{o}C$ overnight before plating cells.

Reactions involved:

The free aldehyde group of the glutaraldehyde reacts with the amide group of the acrylamide as the gel polymerizes, ensuring proper sticking of the gel to the coverslip. Supho-SANPAH, which is added next, is a hetero-bifunctional crosslinker, consisting of a sulpho-NHS ester and a photoactivable nitrophenylazide. The photoactivable nitrophenylazide group reacts with the PAA at the upper gel surface, thus leaving the NHS group free to bind to the primary amines in Fibronectin.

Dissection and culturing:

Media prepared:

1. Embryonic medium (EM): L-15 containing 1X Penstrep
2. Basic Culture Medium with methocel (BCM + M): L-15 containing 1X Penstrep, 0.6% Methocel, 0.6 mg/ml Glucose, 10% FBS.

Chicken (*Gallus gallus*) eggs of either sex were incubated at 37^{o}C, for 6 days. The embryo was taken out in 1X DPBS, and the spinal cord was dissected out into filtered EM, centrifuged at 3000 rpm, 3 minutes. The supernatant was drained and the cell pellet was resuspended in trypsin (37^{o}C, 15 minutes) for permeabilization, following which the cells were brought into solution by gentle mixing. This was centrifuged again (3000 rpm, 3 min), the supernatant was drained and filtered BCM (with methocel) was added. This cell solution was then plated either on fibronectin coated hydrogels (for bead pulling and traction experiments) or fibronectin and Poly-L-Lysine coated glass bottom plates (for fixed experiments). The final culture volume was made up to 2 ml, and NGF (100 ng/ ml) was added before incubation for 24 hrs at 37^{o}C.

Morphology analysis of Cilio D treated growth cones

Spinal neurons, cultured on glass (coated with 1 mg/ ml PLL and 20 µg/ ml Fibronectin) for 24 hours were treated with either 100 µM Cilio D or an equal volume of DMSO. The four different treatments tried were: 15 min DMSO, 5 min Cilio D, 10 min Cilio D and 15 min Cilio D. Higher times of incubation of Cilio D also was checked, and the four time points used for that was: 60 min DMSO, 20 min Cilio D, 40 min Cilio D, 60 min Cilio D

and 80 min Cilio D. The cultures were fixed after the treatments using a fixative (3.5% Paraformaldehyde and 0.05% Glutaraldehyde in 1X PHEM). The fixative is added by exchanging the culture media with the fixative. The fixative was incubated with the cells at room temperature for 10 minutes, after which three 1X PHEM washes were given with an interval of 15 minutes each. Following this, a 0.05% Triton-X (in 1X PHEM) wash was given for 30 minutes. Further, these were again given 1X PHEM washes thrice in intervals of 15 minutes each. The samples are stored at 4^{o}C, if not imaged immediately.

Imaging:

These were imaged under an inverted Olympus TIRF Microscope equipped with a Hamamatsu CCD camera, under the fluorescence mode. A 100X objective and 1X1 binning was used to capture DIC images of these neurons.

Analysis:

Growth cone area is calculated by drawing boundaries as in the Figure 2.2 (A), including both the lamellipodia and filopodia. Area values are retrieved from ImageJ. Protrusions from the lamellipodial base are counted as filopodia only if they are greater than 2 µm in length. Statistical comparisons between various treatments are done with the same tests as mentioned for bead pulling.

Bead pulling assay:

A bead pulling assay involves the use of fluorescent beads as markers for studying filopodial tip adhesions. Neurons were cultured for 24 hours on fibronectin coated PAA hydrogels with fluorescent beads embedded on the surface.

Drug flow and Imaging:

Cultures were taken out of the 37^{o}C incubator after 24 hours and 1 ml of media was drained out from the sides. The rest of the media was exchanged with non-methocel containing BCM (to allow proper diffusion of drugs) and it was incubated back in 37^{o}C for an hour. Cultures were then taken to an inverted Olympus TIRF microscope

equipped with a Hamamatsu CCD camera, where the ambient temperature (37^{o}C) and humidity were maintained. The 1 ml media was again exchanged with non-methocel containing BCM, this time containing either 100 µM Cilio D (2 µl of 50 mM Cilio D in 1 ml medium) or DMSO (2 µl in 1 ml medium). A growth cone was chosen which had atleast one bead attached to a filopodial tip Figure 2.1 (A), (B). Time series of progression of growth cones were imaged in both DIC (Differentia interference contrast) and red channels (100X objective, binning 2X2, acquisition interval = 6 sec) to see neurons and beads respectively, 20 min after the drug treatment.

Analysis: DIC and RFP channel merged videos are opened using ImageJ, and x-y drift is corrected using the ImageJ plugin 'Image Stabilizer'. Filopodia associated with beads at their tips are numbered as in Figure 2.1 (A). Individual filopodia (and the bead channel associated with them) are cropped out and rotated so that their orientation is as shown in the Figure 2.1 (C). ImageJ plugin 'Particle Tracker 2D/ 3D' is used to track individual beads in the bead channel. The algorithm identifies a 2D Gaussian associated with the bead in each image so that bead movement at a sub-pixel resolution can be identified. This is necessary since the beads themselves are 200 nm in diameter and the displacements could be much less than this value. The plugin gives a video of the specified bead tracked in time, allowing a visual cross verification for the user just to make sure that only the desired bead is being tracked. It also gives as output the x-y coordinates of the bead in each image. Only the x coordinates are considered, since the filopodium is already aligned along the x direction. These x coordinates are used to identify peaks and troughs of bead movement in time with respect to its initial position, which are further used to calculate load stepsizes, velocities and the number of pulling events in Microsoft Excel 2007.

Statistics:

All plots are made using GraphPad Prism. Box plots with whiskers are designed according to Tukey method. Mann-Whitney test (with a confidence interval of 95%) was used to compare between different treatments. The bottom boundary of the boxplots are the first quartile and the top boundary corresponds to the third quartiles. The whiskers represent 1.5 times the inter-quartile range of the upper and lower quartiles. The data

that lie beyond the whiskers are termed outliers, and they are shown as points beyond the whiskers.

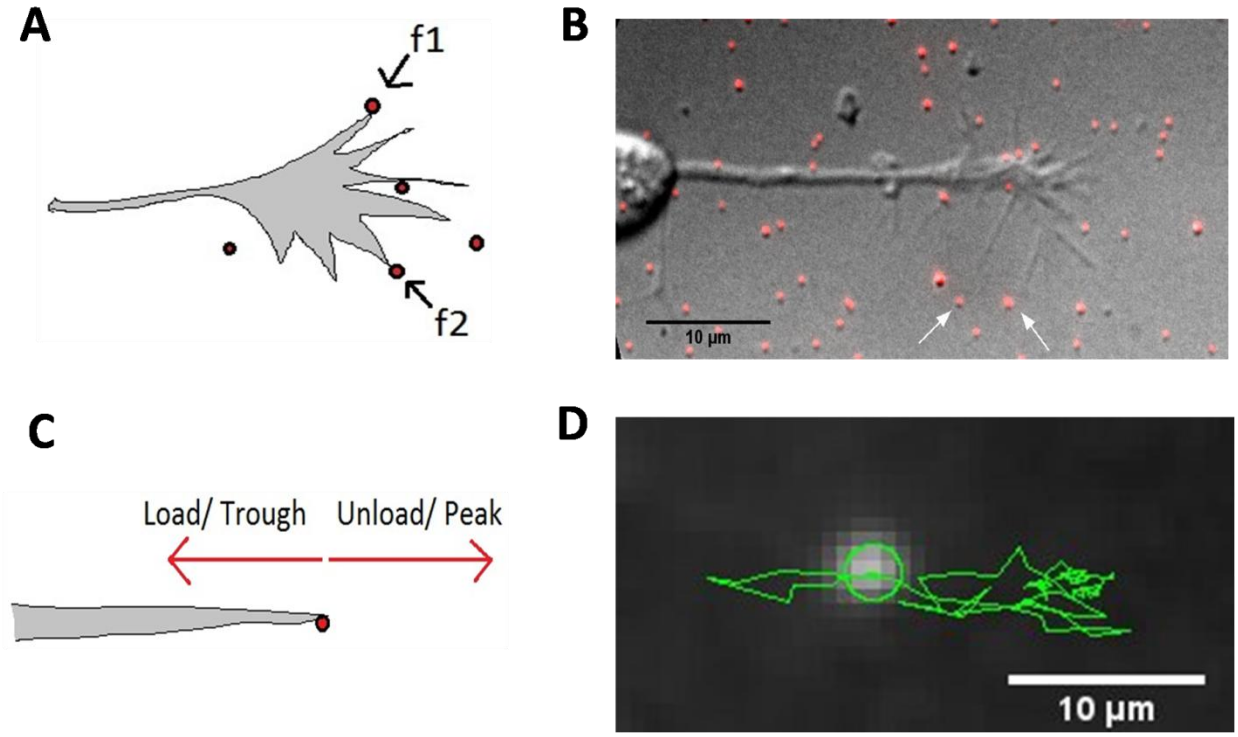

Figure 2.1

Cartoon representation and real images of filopodial pulling and analysis. (A) represents a cartoon of a growth cone, with beads near it. It is shown how to number only the beads at the filopodial tips. (B) is the image of a real neuron, where identification of prospective beads was done. (C) shows how to align filopodia along the x axis and how bead pulling (load) becomes a trough and bead release becomes a peak in the x value with respect to their initial position.

Traction Force Assay

We use the protocol as is used in (Butler et. al.2002) Traction assay is used to calculate force exerted by a cell on its substrate. Trypsin is used to dissociate cells from the ECM protein Fibronectin via its proteolyitc action. For this assay, we require a higher bead density as compared to bead pulling. Hence 20 µg/ ml Fibronectin was layered onto the 18 mm coverslip covering it completely, incubated at 37^{o}C for 30 minutes. Further, this fibronectin was removed from the coverslip using a pipette and bead coating (50 µl of

1:100 (v/v) bead solution) was done following the procedure in Bead pulling assay. The bead density of the traction assay and bead pulling assay are shown in Figure 2.2 (B).

Imaging:

Cultures were taken out of the 37^{o}C incubator after 24 hours and 1 ml of media was drained out from the sides. The rest of the media was exchanged with EM and it was incubated back in 37^{o}C for an hour. This exchange to a non-methocel non-serum containing medium ensures proper diffusion of the drug (Cilio D/ DMSO) and prevention of trypsin deactivation respectively. Cultures were then taken to an inverted Olympus TIRF microscope equipped with a Hamamatsu CCD camera, where the ambient temperature (37^{o}C) and humidity were maintained. The 1 ml media was again exchanged with EM, this time containing either 100 µM Cilio D (2 µl of 50 mM Cilio D in 1 ml medium) or DMSO (2 µl in 1 ml medium). A free growth cone was chosen which had abundant beads next to it and a DIC and RFP image of the same was taken. After 20 min of the drug treatment, 1ml of 10X Trypsin was added to the culture dish (making it an effectively 5X trypsin concentration) and the growth cone was allowed to de-adhere. Both DIC and RFP images (100X objective, 1X1 binning) of the growth cone were taken Before addition of Cilio D / DMSO, 10 min after addition of Cilio D / DMSO, 20 min after addition of Cilio D / DMSO (just before trypsin addition), At complete de-adhering (after trypsin addition).This has been summarized in the Figure 2.2 (C).

Analysis: Using PIV and FTTC plugins in ImageJ, traction heat maps were drawn. The parameters were standardized for this. The plugin inputs the traction heat map after giving the pixel to um ratio and the elasticity of the gel. Atomic force microscopy quantified by Tse and Engler, 2010 calculate the modulus of elasticity of a gel of the fabrication we used, which is reported to be 1.10 ± 0.34 kPa.

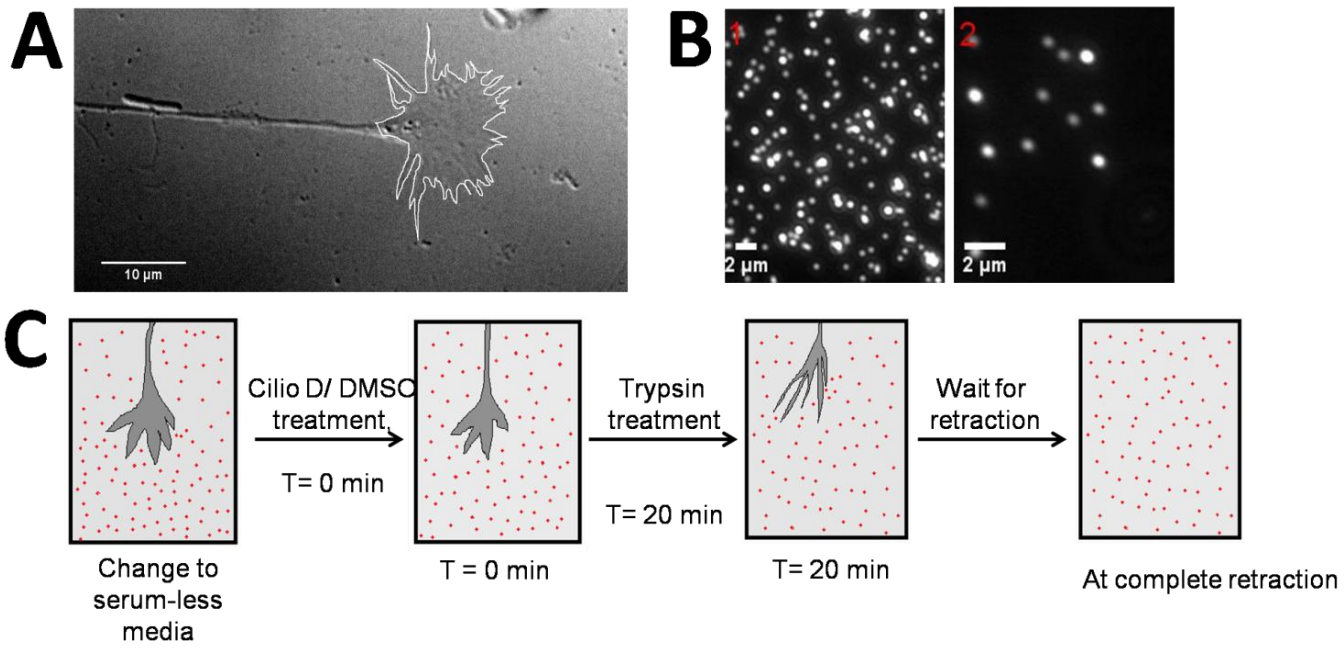

Figure 2.2

Growth cone area estimation and cartoons for traction force microscopy. (A) shows how growth cone areas are measured. (B) shows the difference in bead densities between (1) traction experiment and (2) bead pulling experiment. (C) represents a cartoon for the protocol of traction force microscopy.

Phospho – FAK Staining:

Cells were fixed using the fixation medium used in morphology analysis of Cilio D treated growth cones. They were washed in 1X PHEM four times for 15 minutes each, 1X PHEM Triton for 30 min, !X PHEM four times again (15 minutes each), Blocked in BSA (Bovine serum albumin) for an hour, and primary antibody against P-FAK (dilution 1:1000) was added and kept overnight at 4^{o}C. Again 1X PHEM washes (4 times, 15 minutes each), followed by 1X PHEM Triton washes (30 minutes), 1X PHEM washes (4 times, 15 minutes each), BSA was added (30 min), secondary antibody (1:1000 dilution) was added, kept for half an hour, and then again 1XPHEM washes (4 times, 15 minutes each), BSA was added, Phalloidin (1:200 dilution) was added, 1X PHEM washes (4

times, 15 minutes each) ,1X PHEM Triton wash (30 min), 1X PHEM washes (4 times, 15 minutes each).

Phospho-FAK Quantification:

The growth cone outline was drawn using the free-hand tool, and this region of interest (roi) was saved. ImageJ was used to 'subtract background' from the red channel, following which a gaussian filter was added to the image. The 'clear outside option' was used to clear all the intensities outside the growth cone outline. Next, a threshold was set to identify areas occupied by focal adhesions, and the particles were analyzed to get the area occupied by them and their integrated density. The total intensity in the growth cone was calculated by adding up all the areas above the set threshold and their raw integrated densities, after which the formula below was used to calculate the total intensity of the growth cone.

Total Intensity in a growth cone =

Raw Integrated density – (Sum of areas of all roi_s X Background mean grey value)

This value was divided by the area of each growth cone to normalize the intensity to area.

Cloning of xMRLC into a pCAG backbone and expression:

Xenopus myosin regulatory light chain (xMRLC) in the backbone pLPCX-GFP was kindly provided by Dr. Guillaume Charras, University College London.

The sequence of xMRLC was available in ncbi (GenBank: BC046702.1), the coding sequence of which was reported to be 519 bp. This sequence was used to design primers both homologous recombination and restriction digestion (Kpn1, Age1) primers. The conditions imposed on the primers were that their length should be 18-20 nucleotides, their G-C content should be around 50%, their melting temperature(T_m) should be between 55^{o}C and 60^{o}C, and they should preferably end with guanine or cytosine.

Restriction digestion primers:

Forward: 5’-GCCAAGGGTACCCGCCACCATGTCCAGCAAAAGAGCAAAG-3’

Reverse: 5’-TGTAGCACCGGTCCGTCATCCTTGTCTTTAGCTCC-3’

Homologous recombination primers:

Forward:

5’-GTCGACGGTACCGCGGGCCCCGCCACCATGTCCAGCAAAAGAGCAAAG-3’

Reverse: 5’-GGTGGCGACCGGTGGATCCCCGTCATCCTTGTCTTTAGCTCC-3’

Primers were reconstituted by dissolving in specified volume of Elution buffer to make a 100µM solution.

A Midiprep was done for the pLPCX_MRLC-GFP using NucleoBond XtraMidiprep Kit, and the RNase was removed using a PCR Purification Kit (Promega). Gradient PCR reactions were carried out using both primer pairs, where only the restriction enzyme primers worked. Hence, the pLPCX_MRLC-GFP and pCAG GFP were separately digested with Age1 and Kpn1 overnight, and PCR purification kit (Promega) was used to purify the same. 0.8% Agarose gel electrophoresis was done to check if the digestion worked. Next, ligation reactions (using T4 DNA Ligase, Promega) were carried out with a vector: insert ratio of 1:3 overnight. These ligation mixtures were then transformed into DH5α cells in a Nutrient Agar plate (with Ampicillin resistance) and the plate was incubated at 37^{o}C for 16 hours. Miniprep was done with some colonies from this plate, and a subsequent PCR with the restriction enzyme primers confirmed positive colonies.

The pCAG_MRLC-GFP was transfected into spinal cells just before plating cells for culturing. The transfection was carried out using a NEPA Gene electroporator in Optimem.

Chapter – 3

Results

Reduction in the number of filopodia per growth cone upon dynein disruption

First and foremost, the activity of Cilio D had to be checked. Since growth morphology is known to be affected upon dynein inhibition using the same drug (Sainath et al. 2014), scoring for growth cone morphologies such as growth cone area and filopodial number would help confirming the activity of the drug.

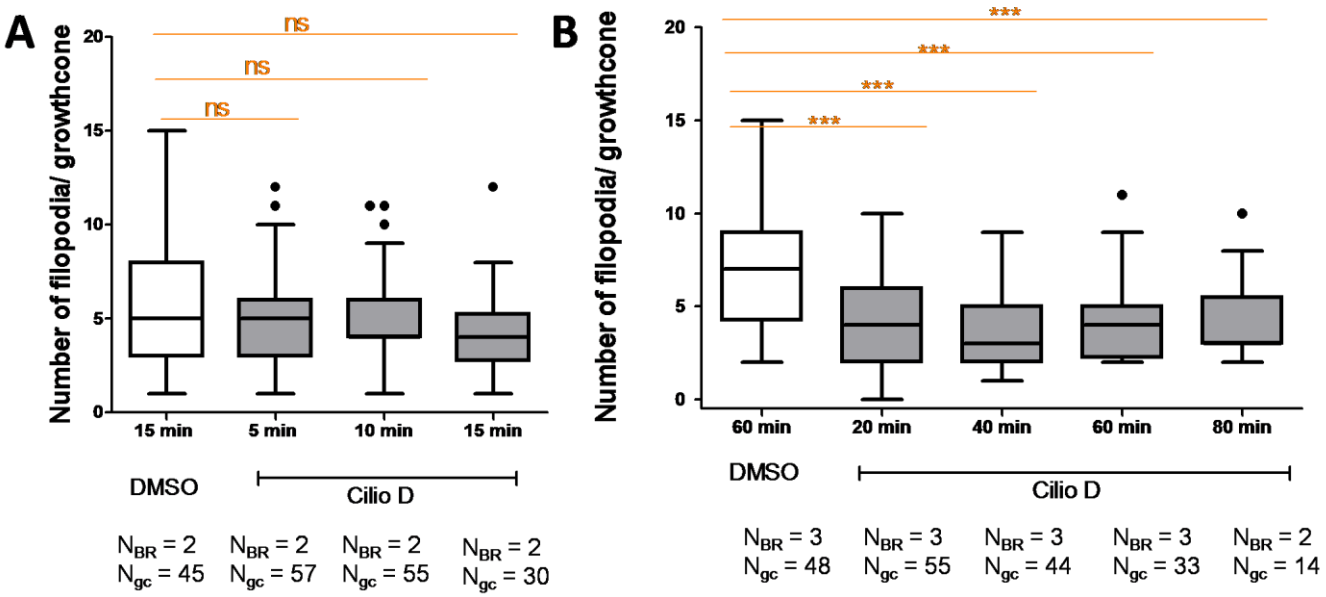

Figure 3.1: Reduction in the number of filopodia per growth cone upon dynein disruption. (A) and (B) show the filopodial numbers per neuron, for cells fixed after 5, 10 and 15 minutes of drug (DMSO/ Cilio D) and 20, 40, 60 and 80 min of drug (Cilio D/ DMSO) respectively. Box plots have whiskers according to Tukey method. A Mann-Whitney two-tailed test, with a confidence interval of 95% (p=0.05) has been done for statistical comparisons. N_{BR} and N_{gc} are the number of biological replicates and growth cones that were analyzed.

A concentration of 100 µM was chosen from literature (Roossien et al. 2014), but the drug incubation time was to be standardized. 24 hours spinal neuronal cultures were subjected to various incubation times in Cilio D for this optimization (5 min, 10 min, 15 min, 20 min, 40 min, 60 min and 80 min) after which they were fixed and the growth cone morphologies were analyzed. Figure 3.1 (A) shows that there is no significant difference in the filopodial numbers at 5 min, 10 min or 15 min treatments of the Cilio D, with reference to the DMSO control. However, Figure 3.1 (B) shows that there is a significant drop (*** = $p<0.001$) in the filopodial numbers per growth cone starting from 20 min after Cilio D treatment, with reference to the DMSO treatment.

Reduction in the growth cone area upon dynein disruption

The same experiment as above was done, and growth cone area has been quantified here as an aspect of growth cone morphology. From Figure 3.2 (A), it can be seen that there is no significant change in the growth cone area till 15 min of 100uM Cilio D treatment. However, from 20 min after Cilio D treatment, there is a significant drop in the growth cone areas.

Dynein disruption does not alter the magnitude or velocity of filopodial pulling

As explained in the objective, filopodial contractility is an important aspect since dynein acts at the periphery of the growth cone, pushing against the membrane. A filopodial bead pulling assay was carried out to investigate if the filopodial contractility was compromised when there was dynein disruption. It can be observed from Figure 3.2 (A) and (B) that there is no significant difference between the DMSO and Cilio D treated growth cones in terms of the filopodial pulling stepsize or the velocity.

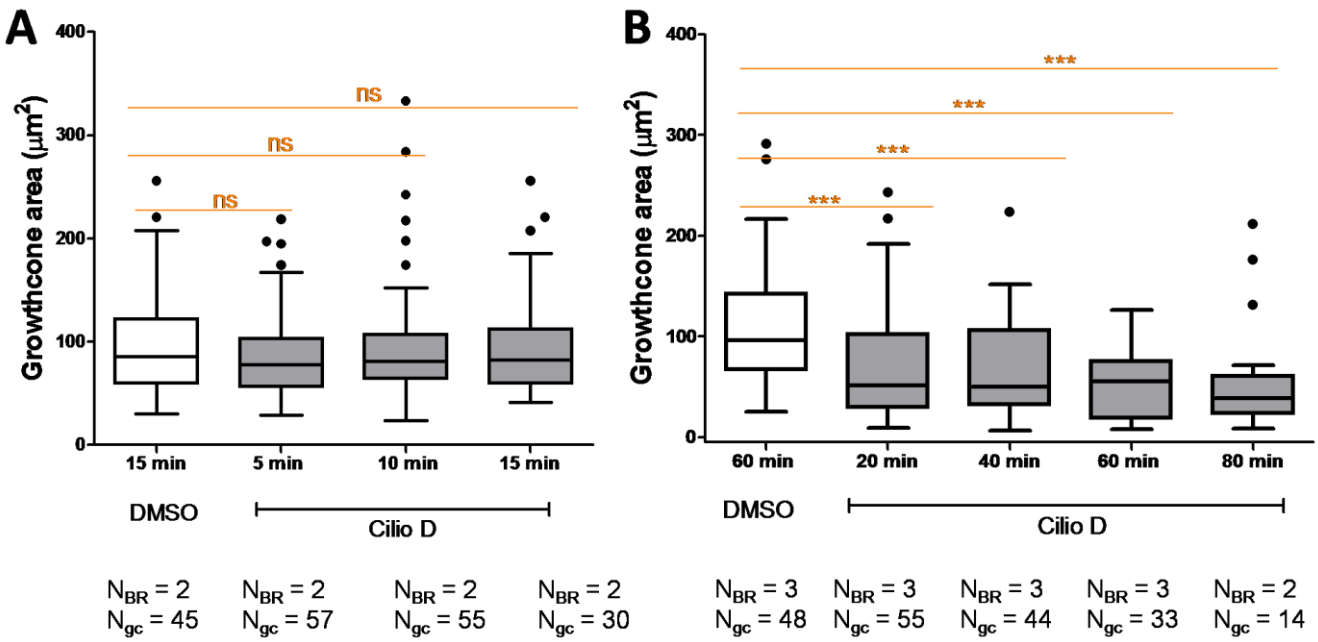

Figure 3.2: Reduction in the growth cone area upon dynein disruption. (A) and (B) show the growth cone areas for cells fixed after 5, 10 and 15 minutes of drug (DMSO/ Cilio D) and 20, 40, 60 and 80 min of drug (Cilio D/ DMSO) respectively. Box plots have whiskers according to Tukey method. A Mann-Whitney two-tailed test, with a confidence interval of 95% (p=0.05) has been done for statistical comparisons. N_{BR} and N_{gc} are the number of biological replicates and growth cones that were analyzed.

Dynein disruption increases the number of filopodial pulling events

Also, at 20 min, the first change in morphology, in terms of both filopodial numbers and growth cone areas were observed. This change in morphology persisted in all the longer incubations. Since dynein disrupted growth cones are observed to retract in live experiments as mentioned in the introduction, a minimum exposure to the drug was to be performed. Otherwise, we would be observing only Cilio D resistant growth cones. The minimum incubation time at which dynein defects in terms of growth cone morphology, was seen at 20 min. Hence, all the experiments henceforth use 20 min as the incubation time. The filopodial bead pulling assay is used here to calculate the number of pulling events each filopodia exhibit per sec. It can be seen clearly from Figure 3.4 that there is an increase in the number of filopodial pulling events per filopodia per sec (**: $p<0.01$).

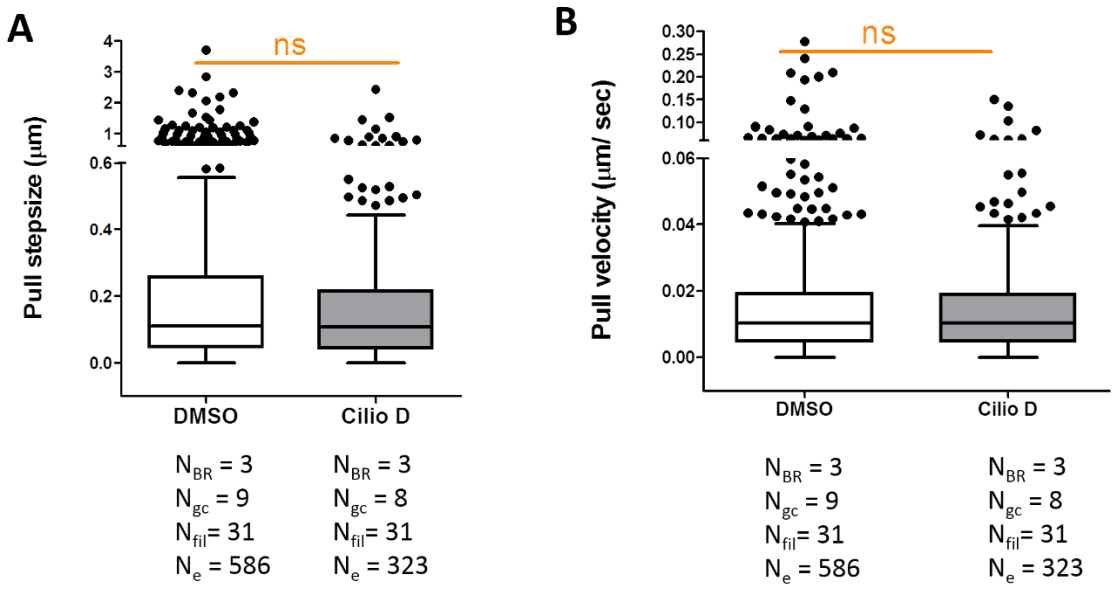

Figure 3.3: Analysis of Bead pulling assay for DMSO and Cilio D treated filopodia. (A) represents the filopodial pulling stepsizes of load/ fail in DMSO and Cilio D treated filopodia. (B) represents the pulling velocity of load/ fail cycles in DMSO and Cilio D treated cells. N_{BR}, N_{gc}, N_{fil} and N_e are the number of biological replicates, growth cones, filopodia and events respectively that were analyzed. Box plots have whiskers according to Tukey method. A Mann-Whitney two-tailed test, with a confidence interval of 95% (p=0.05) has been done for statistical comparisons. N_{BR} and N_{gc} are the number of biological replicates and growth cones that were analyzed.

During dynein inhibition, disassembly of tip adhesions could be responsible for a change in filopodial contractility. Putting this together with data from literature which suggests a complete growth cone retraction upon dynein inhibition (Sainath et al. 2014, Roossien et al. 2014, Roossien et al. 2015), we investigate now if the force generating properties of the whole growth cone is affected. This is performed by Traction force Microscopy.

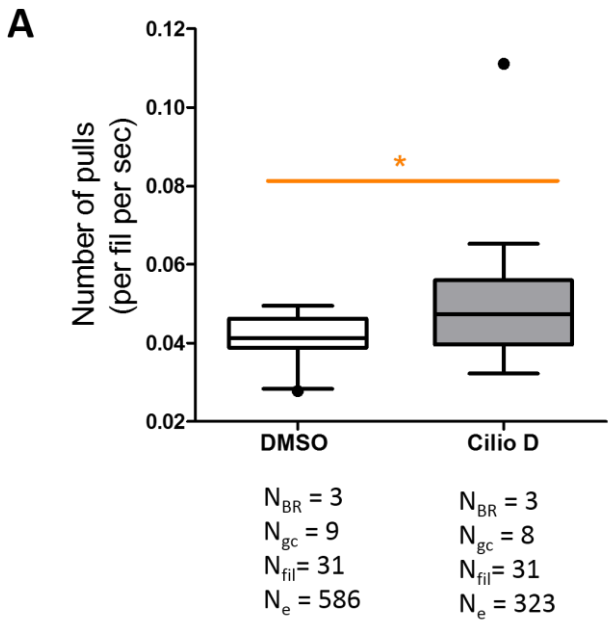

Figure 3.4: Pulling frequencies of filopodial tips increase upon disruption of dynein. (A) shows that there is a significant increase in the filopodial pulling frequency upon Cilio D treatment. N_{BR}, N_{gc}, N_{fil} and N_e are the number of biological replicates, growth cones, filopodia and events respectively that were analyzed. Box plots have whiskers according to Tukey method. A Mann-Whitney two-tailed test, with a confidence interval of 95% (p=0.05) has been done for statistical comparisons.

Traction force assay qualitatively shows lower traction upon dynein disruption

Traction Force Microscopy uses trypsin to de-adhere the growth cone for calculating rms traction. Figure 3.5 (A) and (B) shows the displacement field and the traction forces exerted by cells in a DMSO treated cell. The numbers of growth cones for this experiment are less (nine in DMSO and two in Cilio D). Hence, statistical comparisons between the DMSO and Cilio D treatments cannot be done at this point. However, qualitatively, the traction in the Cilio D treated growth cone looks lower than that of DMSO control growth cone.

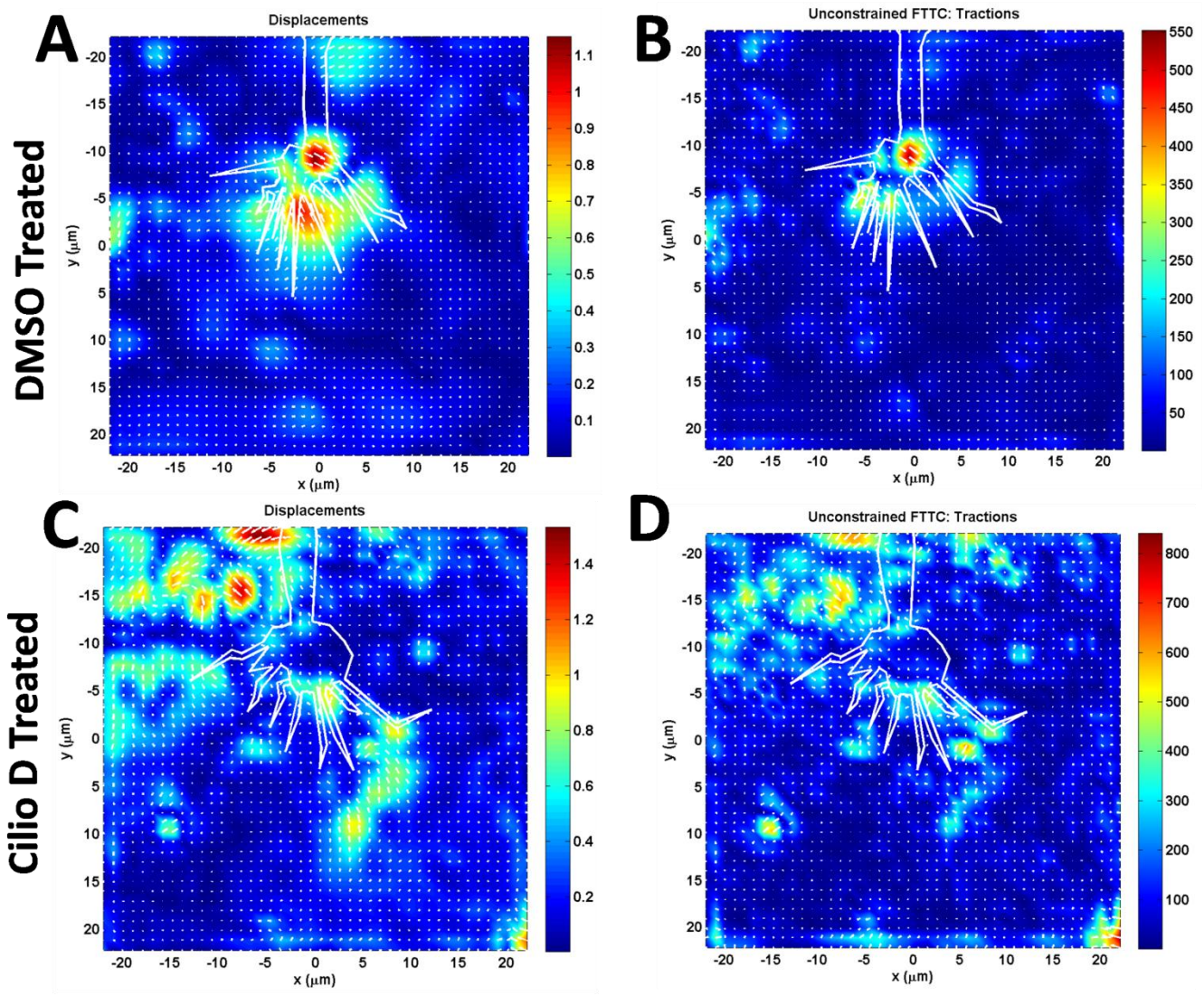

Figure 3.5: Traction force images of neurons. (A) shows the displacement field associated with trypsinization for a DMSO treated growth cone. (B) is the traction force calculated for the same growth cone. (C) and (D) are the displacement and traction maps of a Cilio D treated growth cone.

Intensity of P-FAK staining is lower in dynein inhibited growth cones

As seen from the bead pulling experiment, the filopodial contractility is hampered in dynein depleted growth cones. Also, whole growth cone traction seems to be decreased from the traction force assay. This drop in force generation ability of growth cones can be either due to weakening of point contacts in the dynein depleted scenario. This could

also be due to a change in localization of myosin II, which is the major contractile force generator in the growth cone.

Firstly, we check the abundance/ strength of point contacts upon dynein depletion by staining of P-FAK. As explained in the introduction, FAK is recruited very early upon point contact initiation. FAK is phosphorylated at Y397 (Tyrosine 39) for activation. This is the site of phosphorylation of FAK that has been stained for. The amount of FAK Y397 is a direct measure of the stability of a focal adhesion, since it is a direct consequence of the number of integrins clustered at the surface. This is an important step in downstream signaling for stabilization of the focal adhesions. Hence, P-FAK stains all the point contacts that are actively maturing.

24 hour grown cultures are fixed after various durations of 100 µM Cilio D, and P-FAK and Phalloidin are stained to visualize the point contacts. The Figure 3.6 (A) shows qualitatively the localization and enrichment of point contacts in the growth cone of a DMSO treated cell. The growth cone contains a lot of point contacts, and fewer are present along the length of the filopodia. The next panels Figure 3.6 (B), (C) and (D) show P-FAK staining patterns for 10 min, 20 min and 40 min Cilio D treatments. The staining pattern shows a sparser staining of P-FAK in the growth cone central region compared to the control (Figure 3.6 A). Quantification of this has been shown in Figure 3.7 A, where a clear drop in P-FAK intensity is observed in the set that was incubated for 40 min in Cilio D. Also, in the sets that were incubated in Cilio D for 10 min and 20 min show a drop in P-FAK intensity, but these are not statistically significant.

Cloning and expression of Myosin Regulatory Light Chain (MRLC)

Myosin II is the major contractile force generator in the growth cone (Lin et al., 1996 and Bridgman et al., 2001). Xenopus MRLC (xMRLC) was used as a marker to localize myosin in neurons. The qualitative observations of decreased traction in dynein depleted growth cones from the traction maps and the decrease in P-FAK intensities in dynein disrupted growth cones are consistent in the observation that dynein depletion causes breakage of point contacts and hence could be the reason for the decreased traction forces.

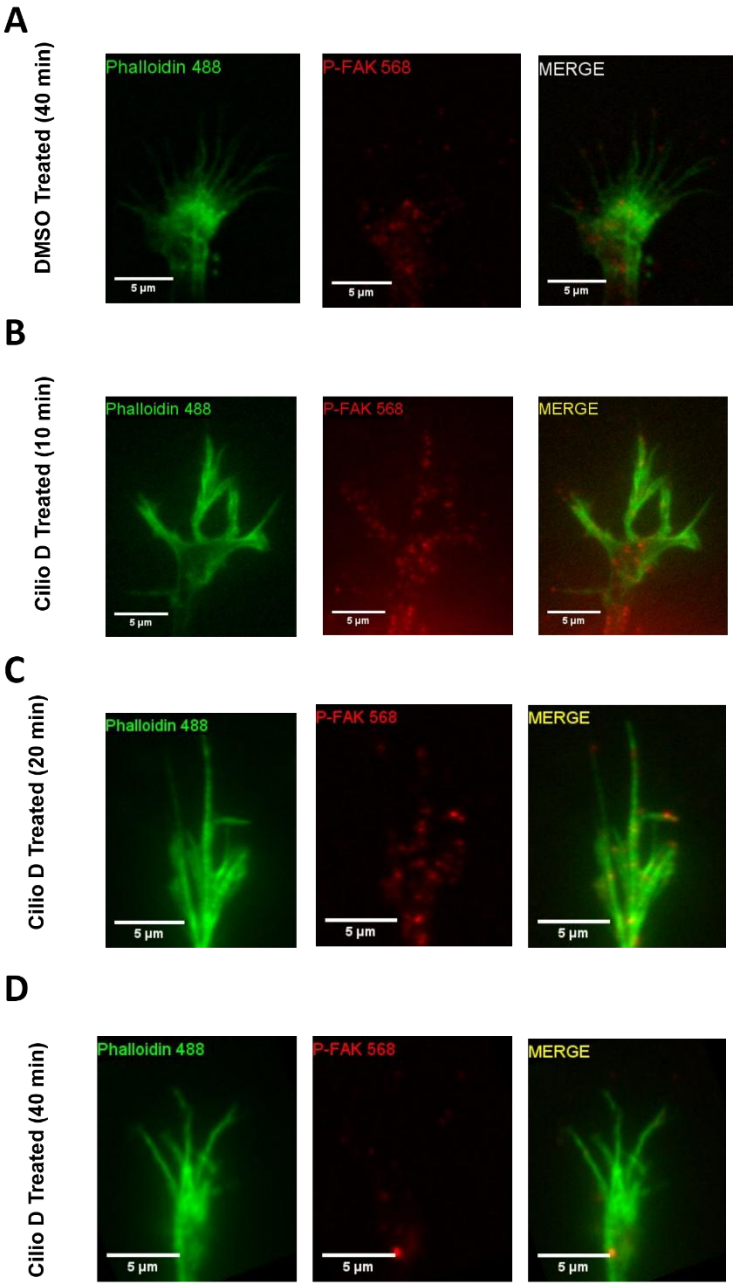

Figure 3.6: Phospho-FAK Staining in neurons after drug treatment (Cilio D/ DMSO). (A) shows the staining pattern of both Phalloidin (green) and Phospho-FAK (red) in a growth cone treated with DMSO, whereas (B), (C) and (D) show the same with a growth cone treated for 10 min with Cilio D.

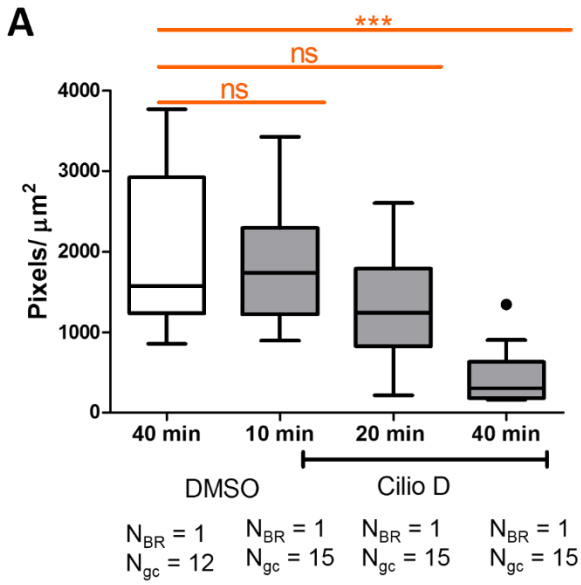

Figure 3.7: Phospho-FAK intensity quantification in DMSO and Cilio D treated neurons. The graph A shows a reduction in the intensity of point contacts in dynein inhibited cells. N_{BR} and N_{gc} are the number of biological replicates and the growth cones respectively that were analyzed. Box plots have whiskers according to Tukey method. A Mann-Whitney two-tailed test, with a confidence interval of 95% (p=0.05) has been done for statistical comparisons.

To investigate what causes the breakage of these attachments, the main candidate to look at, is the contractile force generator in neurons, namely Myosin II. A hypothesis is presented here, which talks about the contractile force of myosin transiently taking over when dynein is inhibited and the force balance between myosin and dynein is disrupted. As myosin pulling increases, there comes a point at which the point contacts break and the growth cone is exerting less force again. The idea is to see if myosin localization somehow changes upon dynein depletion, due to which the force generation could be hampered. To resolve this, myosin activity was localized in growth cones by transfection with a tagged myosin regulatory light chain.

xMRLC was cloned into pCAG-GFP for expression in chick (*Gallus gallus*) cultures. The Figure 3.7 (A) shows PCR products of transformed bacterial DNA run on an agarose gel showing bands for positive colonies obtained at 519 bp, which is the length of the coding sequence of xMRLC. The cloned xMRLC was transfected into spinal neurons, and was imaged under the DIC and GFP filters myosin localization comparisons. It can be seen that myosin is present at the boundary between the P and T domains of the growth cone (Figure 3.7 (B)). Figure 3.7 (C) shows a time lapse of a growth cone visualized under the GFP filter (xMRLC), which again shows that myosin localizes at the boundary of the P and T domains in a dynamic growth cone.

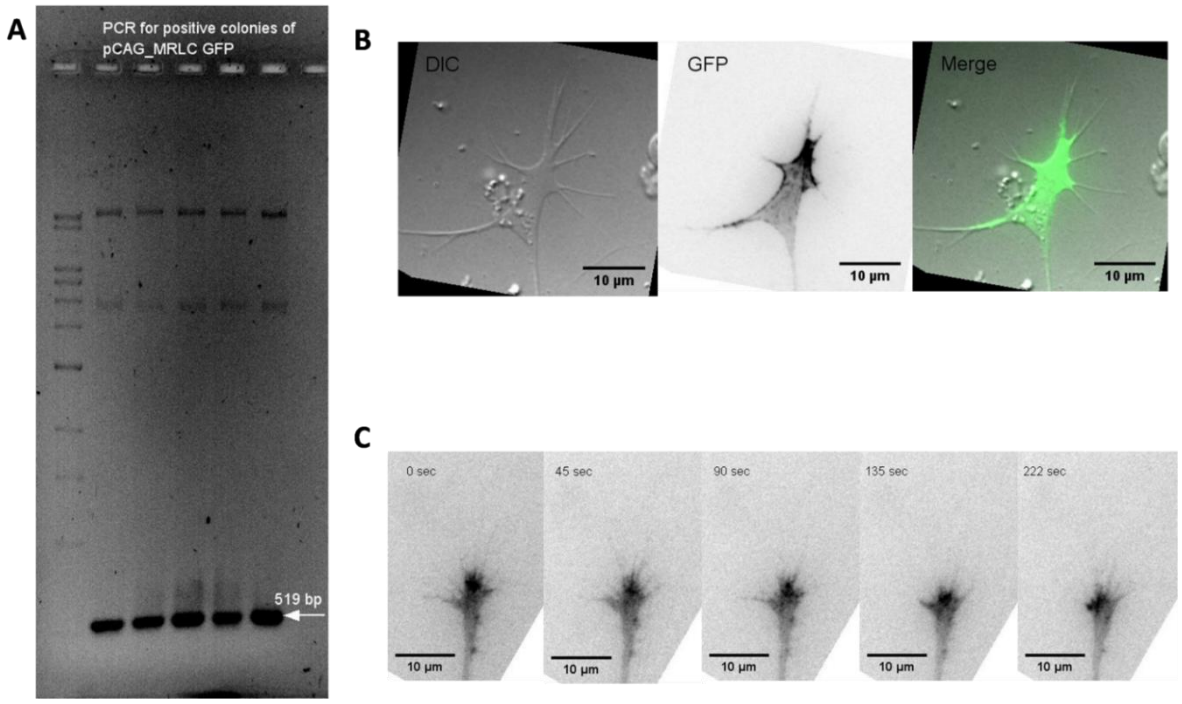

Figure 3.8: xMRLC cloning and expression in chick spinal neurons. (A) shows a 0.8% Agarose gel after electrophoresis. The first well contains Supermix Ladder, and the second, third, fourth, fifth and sixth contain DNA purified from prospective colonies after transformation. There are specific clean bands at 519 bp, indicative of the presence of positive clones in all five colonies. (B) consists of images of neurons cultured for 24 hrs after xMRLC transfection. The DIC and the GFP labeled images are taken under the DIC and GFP channels respectively. The GFP channel image has been inverted. The image labeled 'merge' is a merged channel of the previous two. (C) consists of a timelapse of a neuron expressing xMRLC, showing that the localization pattern of MRLC, which is at the boundary of the P and the C regions, is consistent in a dynamic growth cone.

Chapter 4

Conclusions and Discussion

Cilio D Activity is confirmed in chick spinal neuronal cultures:

Since there is a significant drop in the growth cone area and filopodial numbers, it has been confirmed that Cilio D is active in the cells of choice. Also, in this experiment, the incubation time was optimized to be 20 min.

Sainath et al. 2014 discusses a reduction in filopodial numbers upon dynein disruption 20 min after treatment with 20 µM Cilio D, in agreement with Figure 3.1. They however, do not see a significant change in growth cone area upon treatment with 20 µM Cilio D. Sainath et al. 2014 cultured neurons on glass, whereas this study is done on compliant surfaces. This could be one of the reasons for getting conflicting results. It could also be because they did all experiments in the background of an acute NGF treatment. Also, the Cilio D concentrations that are used in this study have a fivefold higher concentration than theirs.

Dynein inhibition maintains the filopodial pull step sizes and velocities, but increases the frequency of pulls per unit time.

Dynein inhibited growth cones are observed to pull more frequently, even though the pull step sizes and velocities are not significantly different. This could be at least in part due to weakening of point contacts in the growth cone. The dynein inhibited growth cones are not able to sustain more forces. The clutches weaken sooner in these growth cones.

An increase in the frequency of pulling events could mean frictional slippage, described by Chan and Odde, 2008. Frictional slippage occurs on a substrate when the growth cone is not able to generate enough tension to slow F-actin retrograde flow (Chan and Odde 2008). This happens on stiffer substrates, as has been shown by Chan and Odde,

2008. Thus it can be proposed that the growth cones behave as though they are on a stiffer substrate.

The bead pulling analysis can be taken further by sorting the step sizes, velocities and pull times into bins of different frequencies. Some pattern could be there in such distributions.

Dynein inhibited growth cones show a qualitative decrease in traction forces exerted on the substrate

By looking at the heat maps in Figure 3.4, it can be qualitatively noted that the Cilio D treated growth cones pull much less than the DMSO treated ones. The number of cells in this experiment are very low for Cilio D. Hence, the numbers have to be improved to comment on quantitative changes in traction forces upon disruption of dynein.

According to the force balance model for myosin and dynein, if one of them were depleted, the other should take over. Here, when dynein depletion happens, myosin is expected to take over and pull the growth cone even more tightly. In that case, the forces exerted by these growth cones should be larger, contrary to the data observed. This could be because there is some other parameter that dynein is changing. The first candidate could be point contacts. The point contacts could be weaker or fewer in number in the dynein disrupted scenario. Thus, myosin will not be able to pull much since the clutches disengage quicker.

The other factor discussed above responsible for lower traction in growth cones is Myosin II. Myosin itself could be changing localization upon treatment with Cilio D. Thus, myosin localization has to be monitored in dynein depleted neurons. The cloned MRLC transfected neurons have to be Cilio D treated for localizing myosin. Myosin can also be overlaid on traction maps, to investigate whether myosin localization and regions of higher traction force production are the same.

Dynein inhibited growth cones have weaker point contacts

P-FAK staining shows a reduction in its intensity upon Cilio D treatment. Hence, the point contacts are becoming weaker. It has to be noted that this experiment has only

one biological replicate. The numbers have to be improved to comment on the result more convincingly.

Here, a model can be proposed to explain the lower forces qualitatively seen in Cilio D treated growth cones, confirmed by the P-FAK staining quantification. When dynein is inhibited, myosin will dominate as expected. This implies an increase in traction forces, but this could be transient. As myosin pulls on the point contacts, the traction forces increase initially, but since the point contacts in dynein are weaker, they disengage quicker, and hence the overall traction drops down again. Our experiments must be in the regime where the point contacts are already disengaged, which is why a decrease in traction is observed, at least qualitatively.

Traction quantification can be done in time, to see if a transient unbalanced Myosin II pull is observed before the growth cone completely collapses. Myosin disruption using Blebbistatin can be done to observe if transient increase in pulling forces upon dynein disruption. If it is not real, then the intial increase in traction forces will not be observed.

Since the crystal structure of interaction of Cilio D with dynein has not been discovered, it is not completely proven that Cilio D acts only on dynein. Hence, all the above experiments can also be done with another method of dynein disruption, such as siRNA against DHC, etc for confirmation of these results.

References

1. Abe T.K., Honda T., Takei K., Mikoshiba K., Hoffman-Kim D., Jay D.G., Kuwano R. (2008). Dynactin is essential for growth cone advance. Biochemical and Biophysical Research Communications *372(3),* 418–422.
2. Ahmad F.J., Echeverri C.J., Vallee R.B. and Baas P.W. (1998). Cytoplasmic dynein and dynactin are required for the transport of microtubules into the axon. Journal of Cellular Biology *140(2),* 391-401.
3. Ahmad F.J., He Y., Myers K.A., Hasaka T.P., Francis F., Black M.M., Baas PW. (2006). Effects of dynactin disruption and dynein depletion on axonal microtubules. Traffic *7*, 524–537.
4. Ahmad, F. J., Hughey, J., Wittmann, T., Hyman, A., Greaser, M. and Baas, P. W. (2000). Motor proteins regulate force interactions between microtubules and microfilaments in the axon. Nature Cell Biology *2*, 276-280.
5. Aplin J.D. and Hughes R.C. (1981). Protein derivatised glass coverlsips for the study of cell-to-substratum adhesion. Analytical Biochemistry*113,* 144-148.
6. Athamneh A.I.M. and Suter D.M. (2015) Quantifying mechanical force in axonal growth and guidance. Frontiers in Cellular Neuroscience *9,* 359.
7. Baas PW, Black MM, Banker GA. 1989. Changes in microtubule polarity orientation during the development of hippocampal neurons in culture. J Cell Biol 109:3085–3094.
8. Bornschlogl T. (2013). How Filopodia Pull: What We Know About the Mechanics and Dynamics of Filopodia. Cytoskeleton 70, 590–603.
9. Bridgman P.C. and Dailey M.E. (1989). The Organization of Myosin and Actin in Rapid Frozen Nerve Growth Cones. The Journal of Cell Biology *108*, 95-109.
10. Butler J.P., Marija I., Tolic-Nørrelykke, Fabry B., and Fredberg. J.J. (2002). Traction fields, moments, and strain energy that cells exert on their surroundings. Am J Physiol Cell Physiol *282:* C595–C605.

11. Castillo U., Winding M., Lu W. and Gelfand V.I. (2015). Interplay between kinesin-1 and cortical dynein during axonal outgrowth and microtubule organization in *Drosophila* neurons. eLife *4,* e10140.
12. Chan, C.E. and Odde, D.J.(2008). Traction Dynamics of Filopodia on Compliant Substrates. Science *322*, 1687-1691.
13. Dehmelt L., Nalbant P., Steffen W. and Halpain S. (2006). A microtubule-based, dynein-dependent force induces local cell protrusions: Implications for neurite initiation. Brain Cell Biology *35*, 39–56.
14. Engler, A. J., Sen, S., Sweeney, H. L. and Discher, D. E. Matrix elasticity directs stem cell lineage specification. Cell 126, 677–689 (2006).
15. Firestone, A.J., Weinger, J.S., Maldonado, M., Barlan, K., Langston, L.D., O'Donnell, M., Gelfand, V.I., Kapoor, T.M. and Chen, J.K. (2012). Small-molecule inhibitors of the AAA+ ATPase motor cytoplasmic dynein. Nature *484 (7392),* 125–129.
16. Franze K., Gerdelmann J., Weick M., Betz T., Pawlizak S., Lakadamyali M., Bayer J., Rillich K., Gogler M., Lu Y., Reichenbach A., Janmey P. and Kas J. (2009). Neurite Branch Retraction Is Caused by a Threshold-Dependent Mechanical Impact. Biophysical Journal, 97(7), 1883-1890.
17. Geiger B, Spatz JP and Bershadsky A.D. (2009). Environmental sensing through focal adhesions. Nature Reviews Molecular Cell Biology *10(1),* 21-23.
18. Gennerich, A. and Vale, R.D. (2009). Walking the walk: how kinesin and dynein coordinate their steps. Current Opinion in Cell Biology *21,* 59–67.
19. Gomez, T.M., Roche, F.K. and Letourneau, P.C. (1996). Chick sensory neuronal growth cones distinguish fibronectin from laminin by making substratum contacts that resemble focal contacts. Journal of Neurobiology *29*, 18–34.
20. Grabham P.W., Seale G.E., Bennecib M., Goldberg, D.J. and Vallee R.B. (2007). Cytoplasmic dynein and lis1 are required for microtubule advance during growth cone remodeling and fast axonal outgrowth. The Journal of Neuroscience, *27(21),* 5823–5834.
21. Hasaka T.P., Myers K.A., Baas P.W. (2004). Role of actin filaments in the axonal transport of microtubules. Journal of Neuroscience *24(50),* 11291–11301.

22. He, Y., Francis, F., Myers, K.A., Yu, W., Black, M.M., Baas, P.W. (2005). Role of cytoplasmic dynein in the axonal transport of microtubules and neurofilaments. The Journal of Cell Biology *168(5)*, 697–703.
23. Heidemann, S.R., Landers, J.M. and Hamborg, M.A. (1981). Polarity orientation of axonal microtubules. The Journal of Cell Biology *91*, 661-665.
24. Kikkawa, M. (2013). Big steps toward understanding dynein. Journal of Cell Biology *202*, 15- 23.
25. Lin, C. H., Espreafico, E. M., Mooseker, M. S. and Forscher, P. (1996). Myosin drives retrograde F-actin flow in neuronal growth cones. Neuron *16*,769 -782.
26. Lowery, L.A. and Van Vactor, D. (2009). The trip of the tip: understanding the growth cone machinery. Nature Reviews. Molecular Cell Biology *10*, 332–343.
27. Lu,W., Fox, P., Lakonishok, M., Davidson, M.W. and Gelfand, V.I. (2013). Initial neurite outgrowth in drosophila neurons is driven by kinesin-powered microtubule sliding. Current Biology *23*, 1018-1023.
28. Mattila, P.K. and Lappalainen P. (2008). Filopodia: Molecular architecture and cellular functions. Nature Reviews Molecular Cell Biology 9(6), 446-454.
29. Medeiros, N.A., Burnette, D.T. and Forscher, P. (2006). Myosin II functions in actin-bundle turnover in neuronal growth cones. Nature Cell Biology *8(3),* 215-226.
30. Murphey R.K., Caruccio P.C, Getzinger M., Westgate P.J and Phillis R.W. (1999). Dynein–Dynactin Function and Sensory Axon Growth during *Drosophila* Metamorphosis: A Role for Retrograde Motors. Developmental Biology *209(1)*, 86-97.
31. Myers, J.P., Santiago-Medina, M. and Gomez,T.M. (2011). Regulation of axonal outgrowth and pathfinding by integrin-ECMinteractions. Dev Neurobiol. *71(11),* 901–923.
32. Myers, K.A., Tint, I., Nadar, C.V., He, Y., Black, M.M. and Baas, P.W. (2006). Antagonistic Forces Generated by Cytoplasmic Dyneinand Myosin-II during Growth Cone Turning andAxonal Retraction. Traffic *7*, 1333–1351.
33. Sulpho-SANPAH – ThermoFischer Manual

34. Robles, E. and Gomez, T.M. (2006). Focal adhesion kinase signaling at sites of integrin mediated adhesion controls axon pathfinding. Nature Neuroscience *9(10),* 1274-1283.
35. Robles, E., Woo, S. and Gomez, T.M. (2005). Src-dependent tyrosine phosphorylation at the tips of growth cone filopodia promotes extension. Journal of Neuroscience *25*, 7669–7681.
36. Rochlin M.W., Itoh K., Adelstein R.S., Bridgman P.C. (1995). Localization of myosin II A and B isoforms in cultured neurons. Journal of Cell Science *108*, 3661-70.
37. Roossien D.H., Lamoureux P. and Miller K.E. (2014). Cytoplasmic dynein pushes the cytoskeletal meshwork forward during axonal elongation. Journal of Cell Science *127*, 3593–3602.
38. Rosse C., Boeckeler K., Linch M., Radtke S., Frith D., Barnouin K., Morsi A.S., Hafezparast M., Howell M. and Parker P.J. (2012). Binding of dynein intermediate chain 2 to paxillin controls focal adhesion dynamics and migration. Journal of Cell Science *125*, 3733–3738.
39. Sainath R. and Gallo G. (2014). The Dynein Inhibitor Ciliobrevin D Inhibits the Bidirectional Transport of Organelles Along Sensory Axons and Impairs NGF-Mediated Regulation of Growth Cones and Axon Branches. Developmental Neurobiology *75(7),* 757-777.
40. Schnapp B.J. and Reese T.S. (1989). Dynein is the motor for retrograde axonal transport of organelles. PNAS *86(5),* 1548-1552.
41. Suter, D.M. and Forscher, P.(2001). Transmission of growth cone traction force through apCAM – cytoskeletal linkages is regulated by Src family tyrosine kinase activity. The Journal of Cell Biology *155(3)*, 427–438.
42. Tsai, J.W., Bremner, K.H. and Vallee, R.B (2007). Dual subcellular roles for lis1 and dynein in radial neuronal migration in live brain tissue. Nature Neuroscience *10,* 970-979.
43. Tse J.R. and Engler A.J. (2010). Preparation of hydrogel substrates with tunable mechanical properties. Current Protocols in Cell Biology, Chapter 10, Unit 10.16.

44. Wu, D.Y. and Goldberg, D.J. (1993). Regulated tyrosine phosphorylation at the tips of growth cone filopodia. Journal of Cell Biology *123*, 653–664.
45. Zhang, X.F., Schaefer, A.W., Burnette, D.T., Schoonderwoert, V.T. and Forscher, P. (2003). Rho-dependent contractile responses in the neuronal growth cone are independent of classical peripheral retrograde actin flow. Neuron *40*, 931–944.